Solar Energy Materials & Solar Cells 94 (2010) 803–811

Contents lists available at ScienceDirect

Solar Energy Materials & Solar Cells

journal homepage: www.elsevier.com/locate/solmat

Donor–acceptor complex formation in evaporated small molecular organic photovoltaic cells

Diana K. Susarova [a], Pavel A. Troshin [a,*], Doris Höglinger [b], Robert Koeppe [b], Sergey D. Babenko [c], Rimma N. Lyubovskaya [a], Vladimir F. Razumov [a], N. Serdar Sariciftci [b]

[a] Institute of Problems of Chemical Physics of Russian Academy of Sciences, Semenov Prospect 1, Chernogolovka, Moscow 142432, Russia
[b] Linz Institute for Organic Solar Cells (LIOS), Johannes Kepler University Linz, Altenbergerstrasse 69, A-4040 Linz, Austria
[c] Institute for Energy Problems of Chemical Physics, Russian Academy of Sciences (Branch), Semenov Prospect 1/10, Chernogolovka, Moscow 142432, Russia

ARTICLE INFO

Article history:
Received 15 October 2009
Received in revised form
20 December 2009
Accepted 25 December 2009
Available online 8 February 2010

Keywords:
Solar cells
Photovoltaics
Organic semiconductors
Perylene diimides
Naphthalene diimides

ABSTRACT

Novel perylene diimide Py-PDI and naphthalene diimide Py-NDI possessing chelating pyridyl groups have been synthesized. The materials are comparatively investigated as electron acceptors in small molecular photovoltaic cells comprising zinc phthalocyanine ZnPc as an electron donor component. It was shown that these compounds form self-assembled coordination complexes with ZnPc in solution and co-evaporated solid blends. Py-PDI and Py-NDI used as electron acceptor materials in photovoltaic cells with donor ZnPc significantly outperform the reference materials, i.e. perylene and naphthalene diimides that possess no chelating pyridyl groups. Superior photovoltaic performance of Py-PDI and Py-NDI is explained by a complex formation between these compounds and ZnPc. Such interactions of donor and acceptor materials strongly improve photoinduced charge carrier generation. This gives great advantages not just for the construction of organic solar cells but also for organic photodetectors. The devices fabricated in this study are also useful as fast and highly sensitive photodetectors with response times of less than 10 microseconds as well as a strong photoconductive behavior under forward bias.

1. Introduction

One of the most popular research directions in material science is related to the development of cheap and flexible photovoltaic cells comprising thin organic semiconductor films [1–3]. The availability of appropriate soluble materials such as conjugated polymers and fullerene derivatives provides a very exciting opportunity to use high throughput printing technologies for production of organic photovoltaic devices [4–6]. However, there is another promising branch of organic photovoltaics which deals mostly with insoluble low molecular weight organic semiconductors that are deposited by vacuum sublimation or similar techniques that can also be very promising [7–11]. The strongest advantage of small molecular materials is their defined molecular structures and compositions which are virtually not attainable for polymers. Compositional purity of semiconductor materials is a very important issue that must be addressed in order to achieve reproducible characteristics and long term stability in devices. The possibility of attaining a very high degree of chemical purity by vacuum sublimation is a great advantage in using small molecular organic semiconductors.

Many small molecular organic semiconductors are commercially available on a large scale; a number of others are routinely prepared and purified on laboratory scale. In particular, readily available metal phthalocyanines (Fig. 1) are materials of choice for the light absorbing layer in organic photovoltaic devices because of their strong absorption coefficient of $\sim 10^5$ cm^{-1} over a wide range of the solar irradiation spectrum, their high photochemical stability and their charge transport properties. The phthalocyanines as electron donors are combined with materials having high electron affinity, such as fullerene C_{60} or perylene derivatives as electron acceptors. Organic solar cells based on metal phthalocyanines and C_{60} demonstrated power conversion efficiencies of 3–4% comparable with the performances of the polymer/fullerene bulk heterojunctions [6,12].

We have demonstrated recently that the performance of bilayer organic solar cells can be improved dramatically if electron donor and electron acceptor components can form self-assembled complexes at the interface between the layers [13]. This effect was studied in detail using a model system with zinc phthalocyanine (ZnPc) as electron donor material and soluble fullerene derivatives bearing chelating pyridyl groups as electron acceptor component [14].

Another class of small molecular n-type materials for organic electronics is represented by perylene diimides (PDIs) and naphthalene diimides (NDIs) (Fig. 1) [15]. These compounds show excellent environmental stability in organic field effect transistors (OFETs) even without special encapsulation or other protection from air. A combination of copper phthalocyanine and a perylene derivative was used to design the first efficient organic bilayer photovoltaic cell

* Corresponding author. Tel./fax: +7 496 522 1852.
E-mail addresses: troshin2003@inbox.ru, troshin@cat.icp.ac.ru (P.A. Troshin).

0927-0248/$ - see front matter © 2010 Elsevier B.V. All rights reserved.
doi:10.1016/j.solmat.2009.12.027

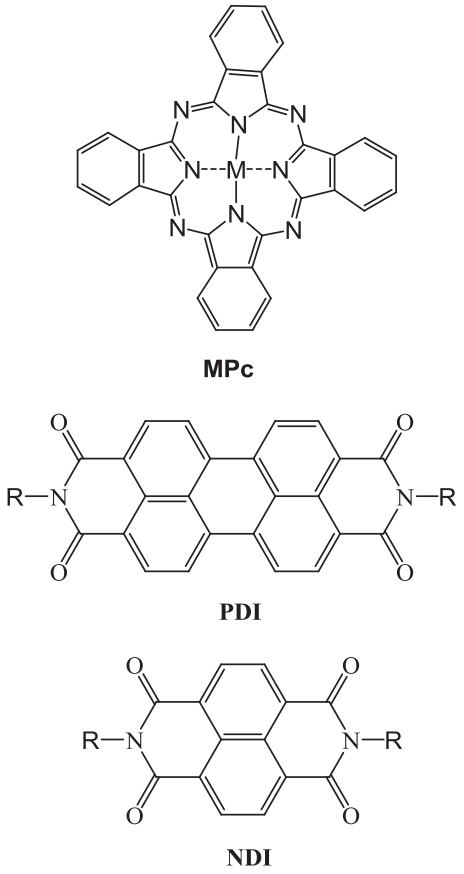

Fig. 1. General representation of the molecular structures of metal phthalocyanine (MPc), substituted perylene diimide (PDI) and naphthalene diimide (NDI).

by Tang in 1986 [9]. Very similar material combinations are studied intensively nowadays with a purpose to design fast organic photodetectors for various applications [16–20].

The absorption spectra of PDIs and NDIs are much different from those of fullerenes, which can lead to additional benefits of their use in combination with phthalocyanines. PDI has a strong absorption band in the green part of the spectrum, exactly covering the absorption gap between the soret- and Q-band of the phthalocyanines. Thus, a solar cell or photodetector made from PDI and phthalocyanines can have high conversion efficiencies over the whole visible spectrum from 400 to 700 nm. NDI is only absorbing in the deep blue and UV, so that the absorption gap of the phthalocyanines allows a high light transmission, so organic solar cells highly transmissive in the visible might become feasible.

In this work we designed novel perylene and naphthalene diimides comprising chelating pyridyl groups in their molecular frameworks and investigated the effect of their complex formation with ZnPc in bilayer photovoltaic devices.

2. Experimental

2.1. Materials and instrumentation

All reagents and solvents were purchased from Acros Organics or Aldrich and used as received. Zinc phthalocyanine was obtained from Chemos GmbH and purified by recrystallization after vacuum sublimation.

The absorption spectra were recorded with a Varian 3G UV–vis spectrophotometer. Photoluminescence spectra were measured with a MUT GmbH Tristan light fiber spectrometer using monochromated light (375 nm) from a 900 W Xe lamp as excitation. The photocurrent spectra were measured with a SRS 830 lockin amplifier using the monochromated light from a 75 W Xe lamp as excitation. *I–V* characteristics were recorded using a Keithley 236 sourcemeter, illumination was provided by a KHS Steuernagel solar simulator calibrated to correspond to 100 mW/cm^2 at AM1.5.

2.2. Synthesis of Py-PDI and Py-NDI

Napthalene-1,4,5,8-tetracarboxylic acid dianhydride (5 g, 16.7 mmol) or perylene-3,4,9,10-tetracarboxylic acid dianhydride (5 g, 12.8 mmol) was mixed with 60 ml of freshly distilled quinoline, 10 g (92.6 mmol) of 3-picolylamine and ca. 100 mg of $Zn(OAc)_2H_2O$. The resulting mixture was heated at reflux for 24 h, then cooled down to room temperature and concentrated to dryness under vacuum (rotary evaporator, oil bath, 120 °C). The residues were suspended in 50 ml of methanol. Solids insoluble in methanol were filtered off, dried in air and further purified by heating at reflux with 50 ml of methanol for 15 min and then separated by filtration. Refluxing with methanol and isolation by filtration was repeated twice; subsequent drying of the obtained solids in air gave crude samples of Py-PDI and Py-NDI. Further purification was performed by sublimation of Py-NDI at 350–400 °C and Py-PDI at 450–500 °C under reduced pressure of ca. 10^{-2} mbar. The sublimation was repeated 2–3 times to ensure a high purity of the materials. The final yields of purified Py-PDI and Py-NDI were ca. 45–50%.

2.2.1. Py-PDI

NMR data were not obtained due to complete insolubility of the material. Chemical analysis: $C_{36}H_{20}N_4O_4$. Cald: C, 75.52; H, 3.52; N, 9.79. Found: C, 75.28; H, 3.31; N, 9.77. IR spectrum (powder): υ=719, 748, 762, 793, 809, 839, 859, 1031, 1117, 1137, 1184, 1275, 1327, 1344, 1365, 1402, 1435, 1480, 1503, 1578, 1592, 1656, 1687 cm^{-1}.

2.2.2. Py-NDI

^{1}H NMR (400 MHz, $CDCl_3$,) δ=8.82 (br. s, 2H, H–Py), 8.77 (s, 4H, H–Ar), 8.52 (t, 2H, H–Py), 7.89 (d, 2H, H–Py), 7.15 (d, 2H, H–Py), 5.4 (s, 4H, CH_2–Py) ppm. Chemical analysis: $C_{26}H_{16}N_4O_4$ Cald: C, 69.64; H, 3.60; N, 12.49. Found: C, 69.70; H, 3.56; N, 12.61. IR spectrum (KBr pellet): υ=554, 566, 628, 708, 720, 750, 770, 792, 832, 891, 898, 999, 1030, 1096, 1111, 1124, 1178, 1188, 1217, 1231, 1250, 1318, 1335, 1374, 1430, 1452, 1478, 1576, 1592, 1665, 1688, 1702, 3020, 3035, 1666, 1706, 3033, 3066 cm^{-1}.

2.3. Synthesis of Bu-NDI and Bn-NDI

Napthalene-1,4,5,8-tetracarboxylic acid dianhydride (4 g, 13.4 mmol) was mixed with 60 ml of freshly distilled quinoline, 6.54 g (89 mmol) of n-butylamine or 10 g (93 mmol) of benzylamine and ca. 100 mg of $Zn(OAc)_2H_2O$. The resulting mixtures were heated at reflux for 12 h, then cooled down to the room temperature and poured into 600 ml of 10% aqueous HCl. The precipitates formed were filtered off, washed several times with methanol and dried in air. The obtained crude products were dissolved in toluene (800 ml) under heating and poured onto silica gel column (3 × 25 cm, ACROS Organics, 40–60 μm, 60 Å). Elution first with toluene and then with a toluene–methanol mixture (99:1 v/v) yielded purified Bu-NDI and Bn-NDI as bright yellowish solids. Repeated chromatographic purification afforded almost colorless solids of Bu-NDI and Bn-NDI that were further purified by single (Bn-NDI) or double (Bu-NDI) sublimation in vacuum at 350–400 °C under pressure of ca. 10^{-2} mbar. The purified samples of Bn-PDI and Bu-NDI were obtained with ca. 55–60% yields.

2.3.1. Bn-NDI

^{1}H NMR (400 MHz, $CDCl_3$) δ=8.77 (s, 4H, H–Naphth), 7.56 (d, 4H, 2,6-Ph), 7.34 (t, 4H, 3,5-Ph), 7.28 (t, 2H, 4-Ph), 5.40 (s, 4H, CH_2) ppm. ^{13}C NMR (150 MHz, $CDCl_3$) δ=162.83 (C=O), 136.52 (1-Ph), 131.18 (C–Naphth), 129.16 (2,6-Ph) 128.6 (3,5-Ph), 127.87 (4-Ph), 126.72 (C–Naphth), 126.67 (C–Naphth), 44.02 (OCH_2) ppm. Chemical analysis: $C_{28}H_{18}N_2O_4$. Cald: C, 75.33; H, 4.06; N, 6.27. Found: C, 75.39; H, 4.12; N, 6.25. IR spectrum (KBr pellet): υ=457, 544, 562, 630, 698, 712, 738, 748, 760, 768, 810, 825, 882, 890, 892, 966, 970, 983, 994, 1003, 1029, 1074, 1104, 1113, 1183, 1224, 1243, 1330, 1367, 1450, 1495, 1508, 1578, 1604, 1666, 1706, 3033, 3066 cm^{-1}.

2.3.2. Bu-NDI

^{1}H NMR (400 MHz, $CDCl_3$) δ=8.74 (s, 4H, H–Naphth), 4.19 (t, 4H, NCH_2), 1.71 (m, 4H, NCH_2CH_2), 1.44 (m, 4H, $NCH_2CH_2CH_2$), 0.97 (t, 6H, CH_3) ppm. ^{13}C NMR (150 MHz, $CDCl_3$) δ=162.85 (C=O), 130.93 (C–Naphth), 126.67 (C–Naphth), 126.62 (C–Naphth), 40.75 (OCH_2), 30.15 (OCH_2CH_2), 20.34 ($OCH_2CH_2CH_2$), 13.81 (CH_3) ppm. Chemical analysis: $C_{22}H_{22}N_2O_4$ Cald: C, 69.83; H, 5.86; N, 7.40. Found: C, 69.88; H, 6.07; N, 7.44. IR spectrum (powder): υ=697, 711, 738, 748, 760, 768, 811, 825, 887, 895, 984, 996, 1003, 1030, 1075, 1105, 1183, 1215, 1224, 1243, 1291, 1305, 1328, 1367, 1428, 1451, 1496, 1580, 1663, 1704 cm^{-1}.

2.4. Synthesis of Bn-PDI, EH-PDI, and CyHex-PDI

Perylene-3,4,9,10-tetracarboxylic acid dianhydride (5 g, 12.8 mmol) was mixed with 60 ml of freshly distilled quinoline, 10 g (93 mmol) of benzylamine or 15 g (116 mmol) of 2-ethylhexylamine or 10 g of cyclohexylamine (101 mmol) and ca. 100 mg of $Zn(OAc)_2H_2O$. The resulting mixtures were heated at reflux for 12 h, then cooled down to room temperature and poured into 600 ml of 10% aqueous HCl. The precipitates formed were filtered off, washed several times with methanol and dried in air. The obtained crude sample of Bn-PDI was purified by treatment with methanol at reflux (as described above for Py-PDI) and then by double sublimation at 450–500 °C under reduced pressure of ca. 10^{-2} mbar.

Compounds EH-PDI and CyHex-PDI were further purified by column chromatography. For this purpose, 500 mg of the crude material were dissolved in 1 l of dichloromethane and then the resulting solutions were poured onto a silica gel column (3 × 25 cm, ACROS Organics, 40–60 μm, 60 Å). Elution with a CH_2Cl_2–methanol mixture (95.5:0.5 v/v) resulted in pure compounds EH-PDI and CyHex-PDI. Final purification was achieved by sublimation at 450–500 °C under reduced pressure of ca. 10^{-2} mbar. The yields of pure Bn-PDI, EH-PDI, and CyHex-PDI were in the range of 35–55%.

2.4.1. Bn-PDI

^{1}H NMR (400 MHz, $CDCl_3$,) δ=8.75 (d, 4H, H–Ar), 8.68 (d, 4H, H–Ar), 7.60 (d, 4H, *o*-Ph), 7.30 (m, 6H, *m*+*p*-Ph), 5.44 (s, 4H, NCH_2Ph) ppm. Chemical analysis: $C_{38}H_{22}N_2O_4$ Cald: C, 79.99; H, 3.89; N, 4.91. Found: C, 80.17; H, 3.97; N, 4.86. IR spectrum (KBr pellet): υ=486, 636, 667, 694, 745, 809, 852, 999, 1172, 1247, 1299, 1339, 1370, 1402, 1434, 1494, 1557, 1577, 1591, 1660, 1694 cm^{-1}.

2.4.2. EH-PDI

^{1}H NMR (400 MHz, $CDCl_3$,) δ=8.83 (d, 4H, H–Ar), 8.75 (d, 4H, H–Ar), 4.31 (m, 4H, NCH_2), 2.14 (m, 2H, CH), 1.58 (m, 8H, CH_2), 1.50 (m, 8H, CH_2), 1.13 (t, 6H, CH_3), 1.06 (t, 6H, CH_3), ppm. Chemical analysis: $C_{40}H_{42}N_2O_4$. Cald: C, 78.15; H, 6.89; N, 4.56. Found: C, 77.95; H, 6.97; N, 4.61. IR spectrum (KBr pellet): υ=745, 809, 1178, 1247, 1308, 1346, 1380, 1403, 1441, 1577, 1594, 1615, 1650, 1695, 2859, 2873, 2930, 2958 cm^{-1}.

2.4.3. CyHex-PDI

^{1}H NMR (400 MHz, $CDCl_3$,) δ=8.68 (d, 4H, H–Ar), 8.63 (d, 4H, H–Ar), 5.07 (m, 2H, NCH), 3.75 (m, 4H, CH_2), 2.59 (m, 4H, CH_2), 1.96 (m, 4H, CH_2), 1.79 (m, 4H, CH_2), 1.49 (m, 4H, CH_2) ppm. Chemical analysis: $C_{38}H_{38}N_2O_4$ Cald: C, 77.79; H, 6.53; N, 4.77. Found: C, 77.84; H, 6.44; N, 4.75. IR spectrum (KBr pellet): υ=456, 652, 745, 798, 808, 1117, 1181, 1246, 1261, 1270, 1339, 1355, 1405, 1434, 1447, 1575, 1594, 1655, 1694, 2852, 2929 cm^{-1}.

2.5. Preparation of bilayer ZnPc/NDI and ZnPc/PDI photovoltaic devices

A ~60 nm thick film of poly(3,4-ethylenedioxy)thiophene : poly(styrenesulfonate) (PEDOT:PSS) (Baytron P) was spincast on glass substrates (14 × 14 mm) coated with 200 nm indium tin oxide (ITO) and dried by heating at 150 °C in air for 15 min. Zinc phthalocyanine was sublimed in an evaporation chamber at a pressure below 10^{-5} mbar to obtain films with 40 nm thickness. Then 30 nm thick films of corresponding NDI or PDI were sublimed under the same conditions on top of the ZnPc layer. Afterwards, the samples were transferred immediately to an argon glove box; there the deposition of a LiF (ca. 0.9 nm)–Al (100 nm) electrode was carried out under vacuum 10^{-6} mbar in an evaporation chamber integrated in the glove box.

2.6. Preparation of diffuse bilayer ZnPc/ZnPc+PDI/PDI photovoltaic devices

A ~60 nm thick film of poly(3,4-ethylenedioxy)thiophene : poly(styrenesulfonate) (PEDOT:PSS) (Baytron P) was spincast on glass substrates (14 × 14 mm) coated with 200 nm indium tin oxide (ITO) and dried by heating at 150 °C in air for 15 min. Photoactive layers were deposited in Leybold Univex 350 evaporation chamber at a pressure below 10^{-5} mbar. A sublimation of 10 nm of pure ZnPc was followed by co-evaporation of ZnPc and PDI to obtain 45 nm thick composite layers, and finally 20 nm of pure PDI were sublimed on the top. Afterwards, the samples were transferred immediately to an argon glove box; there the deposition of a LiF (ca. 0.9 nm)–Al (100 nm) electrode was carried out under vacuum 10^{-6} mbar in an evaporation chamber integrated in the glove box.

3. Results and discussion

3.1. Preparation of the materials

Compounds Py-NDI and Py-PDI (see Scheme 1) were synthesized in the reactions of 3-picolyamine with napthalene-1,4,5,8-tetracarboxylic acid and perylene-3,4,9,10-tetracarboxylic acid dianhydrides, respectively (Scheme 1). The synthesis was carried out using zinc acetate as a catalyst and quinoline as a solvent; the details are given in Experimental. Using analogous reactions, a few other substituted naphthalene and perylene diimides were prepared in order to obtain sets of similar NDIs and PDIs for comparison (Scheme 1).

The compounds Bu-NDI, Bn-NDI, CyHex-PDI and EH-PDI demonstrated reasonably high solubility in organic solvents. Therefore, column chromatography was applied as a first step of purification using toluene/methanol (Bu-NDI, Bn-NDI) or dichloromethane/methanol (EH-PDI) binary solvent mixtures as eluents.

The next step of purification of Bu-NDI, Bn-NDI and EH-PDI was sublimation in vacuum usually performed twice for each

material. In the case of the insufficiently soluble compounds Py-NDI, Py-PDI, Bn-PDI and CyHex-PDI, vacuum sublimation was the only purification method used. Therefore in the case of these materials, the sublimation procedure was repeated 2–3 times to make sure that a high purity was achieved.

To characterize the prepared compounds, we applied NMR spectroscopy where it was possible to achieve sufficient concentrations of the materials in solutions, IR-spectroscopy and chemical analysis. The obtained analytical data are in a good agreement with the molecular structures shown in Scheme 1 and confirmed the high purity of the materials (numerical data listed in experimental).

3.2. Photoluminescence quenching experiments

The photoluminescence (PL) of ZnPc is quenched by electron deficient molecules such as fullerenes and their derivatives, perylene or naphthalene diimides. Here the ability of three synthesized naphthalene diimides to quench the PL of ZnPc in solution was compared. For this purpose, successively increased amounts of NDIs were added to an aliquot of the ZnPc solution while ZnPc PL was monitored. It was revealed that indeed all three NDIs quench the PL of ZnPc. As example, the decrease in the ZnPc PL intensity upon addition of Py-NDI is illustrated in Fig. 2a.

It is notable that the quenching ability of Py-NDI is much higher than that of two other compounds: Bn-NDI and Bu-NDI. This effect is most evident from the Stern–Volmer graphs where the quenching factor ($I_0/I-1$) is plotted against the molar concentration of the quenchers. The quenching factor $I_0/I-1$ is calculated as a ratio between maximal PL intensities in the spectra of pure ZnPc solution (I_0) and ZnPc solution after addition of the quencher (I) minus 1. A linear dependence between $I_0/I-1$ and the quencher concentration is expected for a purely diffusion driven quenching mechanism. The slope of this linear dependence is called the Stern–Volmer constant K_{sv}, which is directly related to the quenching rate as $K_{sv}=f\tau_f k_q$, where k_q is a quenching rate, and τ_f is a fluorescence lifetime. The experimental points on the Stern–Volmer plots for all three NDIs can be fitted with reasonable accuracy by linear dependences. Therefore, we could apply the above equation to calculate quenching rates k_q. For these calculations we used a value of 3 ns for ZnPc fluorescence lifetime

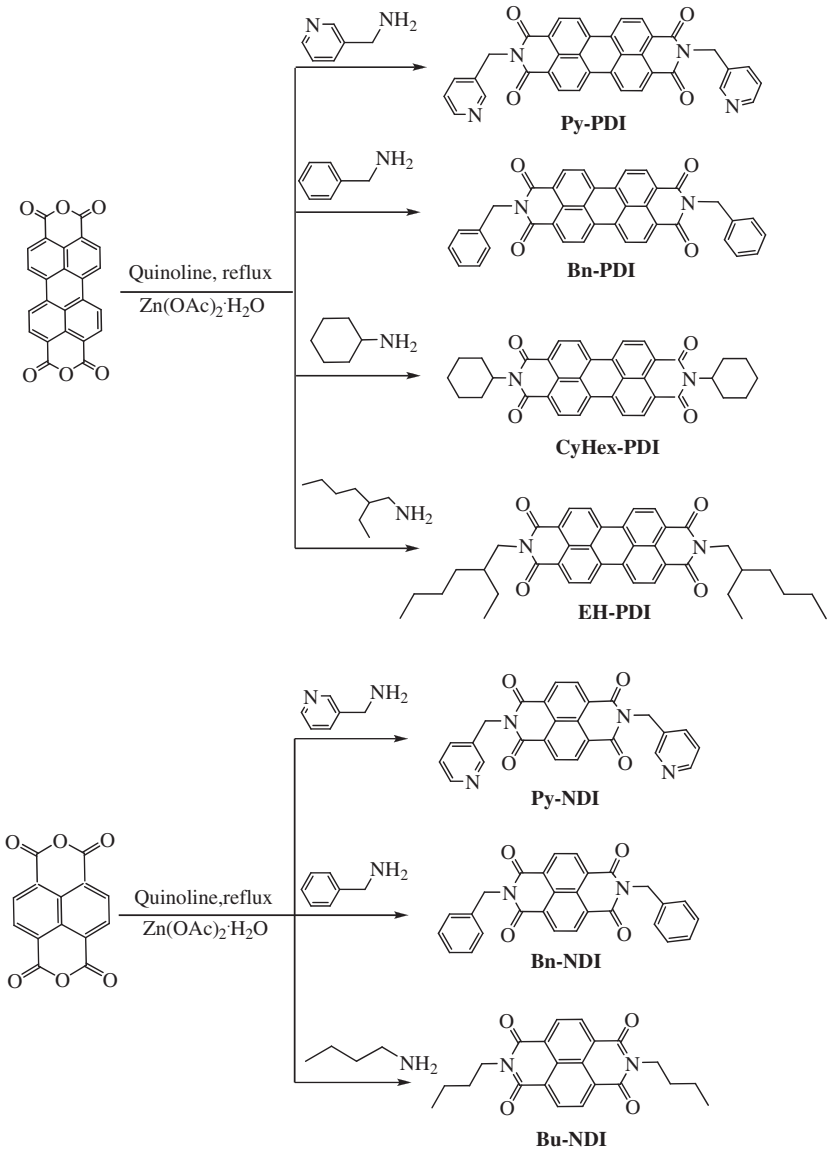

Scheme 1. Synthetic routes used for the preparation of perylene diimides and naphthalene diimides.

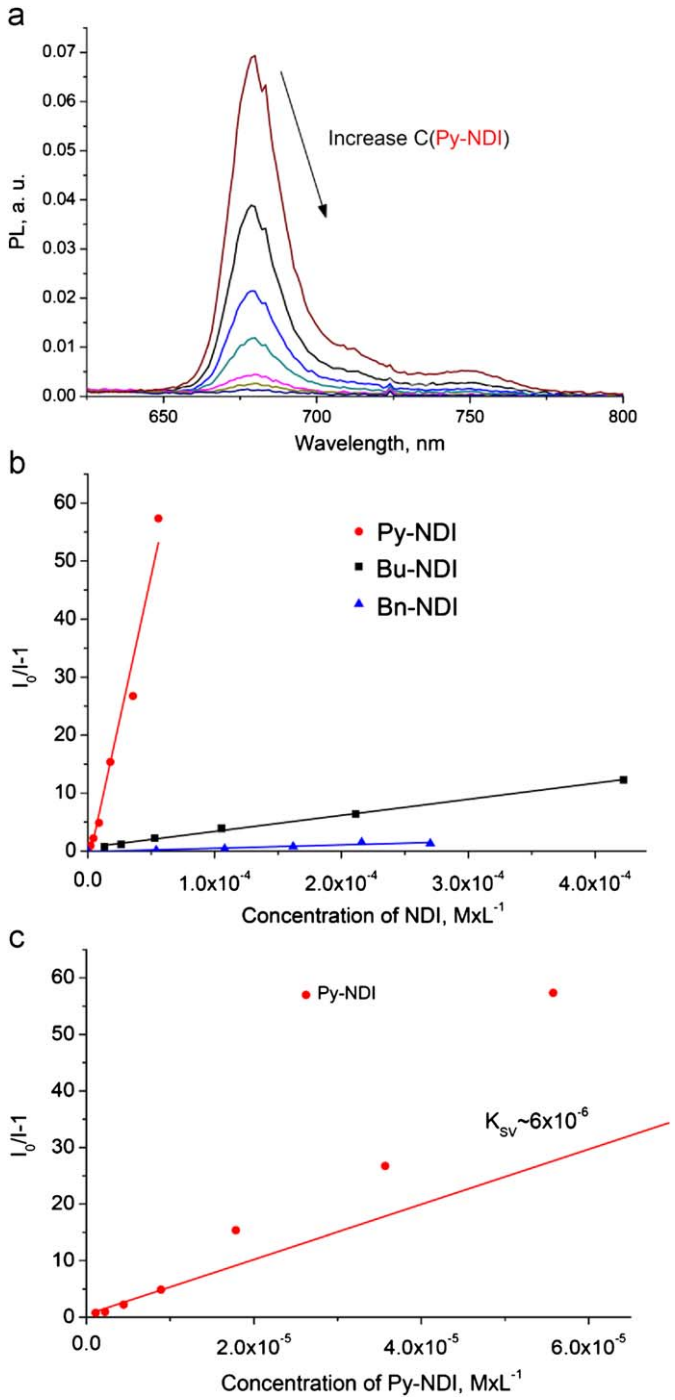

Fig. 2. ZnPc PL quenching upon addition of Py-NDI (a). Stern–Volmer plots illustrating the ZnPc PL quenching by three different NDIs (b). Magnified Stern–Volmer plot illustrating the superlinear behavior of ZnPc PL quenching by Py-NDI (c).

(τ_f) that was reported previously in literature [21]. The obtained results are listed in Table 1.

It can be seen from Table 1 that Py-NDI shows 33 and 188 times higher ZnPc PL quenching rate than Bu-NDI and Bn-NDI, respectively. The remarkably high quenching rate for Py-NDI as compared to other NDIs suggests the existence of intermolecular interactions between Py-NDI and ZnPc that enhance the PL quenching. Based on previous observations on fullerene–zinc phthalocyanine complexations [17]; we propose that Py-NDI forms coordination complexes with ZnPc in solution and that such association results in a more efficient ZnPc PL quenching. We can

Table 1
Stern–Volmer constants and quenching rates for NDIs used as quenchers of the ZnPc PL.

Quencher	K_{sv}, l/mol	k_q, s^{-1}
Py-NDI	9.5×10^6	3.2×10^{15}
Bu-NDI	2.9×10^5	9.7×10^{13}
Bn-NDI	5.0×10^4	1.7×10^{13}

also mention that Py-NDI shows the strongest deviations from a linear behavior in the Stern–Volmer plot (Fig. 2b). These deviations have a superlinear character that is a sign of some association of a fluorescent and a quencher species in solution. Very similar superlinear behavior was observed in our recent studies of ZnPc PL quenching by fullerene derivatives with appended pyridyl groups [22]. A coordination complex formation was proven for this system in solid state and in solution by a number of methods including X-ray crystallography [8,9,23].

The obtained PL quenching data strongly suggest that Py-NDI forms coordination complexes with ZnPc in solutions; this becomes possible due to the presence of chelating pyridyl groups in Py-NDI molecular framework that are known to have a strong affinity to form a complex with Zn^{2+} ions embedded in porphyrin or phthalocyanine macrocycle rings [24].

3.3. *Absorption spectra of co-evaporated ZnPc/NDI and ZnPc/PDI thin films*

We have observed recently that the complex formation between fullerene derivatives bearing chelating pyridyl groups and ZnPc in thin films results in a drastic change of their absorption spectra. In particular, an appearance of a sharp band centered at 690–694 nm was assigned to the coordination complexes formed at a diffused interface between ZnPc and the fullerene derivative [9]. Optical absorption spectroscopy was used here for measurements of a three-layer sandwiches composed of 10 nm of pure ZnPc as bottom-layer, 45 nm of co-evaporated ZnPc:NDI or ZnPc:PDI blend as interlayer and 20 nm of pure NDI or PDI as a top layer. The obtained spectra are shown in Fig. 3. It is clearly seen from this figure that the systems comprising ZnPc and pyridyl-containing compounds Py-PDI and Py-NDI show sharper bands with maxima at 690–694 nm in the spectra suggesting the complex formation between the components.

At the same time, the spectra of the reference systems based on ZnPc and non-chelating NDIs and PDIs also do not fit very well to the superposition of the spectra of individual materials, though the deviations are relatively small in comparison with ZnPc+Py-NDI and ZnPc+Py-PDI composites. The strongest differences are observed in the phthalocyanine absorption region at 550–800 nm. In the spectrum of the pristine phthalocyanine film the left shoulder with maximum at 630 nm dominates over the right shoulder with maximum at 710 nm. On the contrary, in the spectra of co-evaporated films right shoulder is more pronounced than the left one. Such spectral changes might be a consequence of a disturbed π–π stacking of ZnPc molecules by admixed PDI or NDI molecules. Another explanation can be the existence of some intermolecular interactions between ZnPc on the one side and PDIs or NDIs on the other. The latter could be possible via π–π interactions of donors and acceptors since all these molecules are flat and potentially capable of efficient orbital overlapping.

Summarizing this part, we note that two materials possessing pyridyl groups (Py-PDI and Py-NDI) cause strong changes of the ZnPc absorption band, we propose that this effect arises due to a coordination complex formation in co-evaporated thin films.

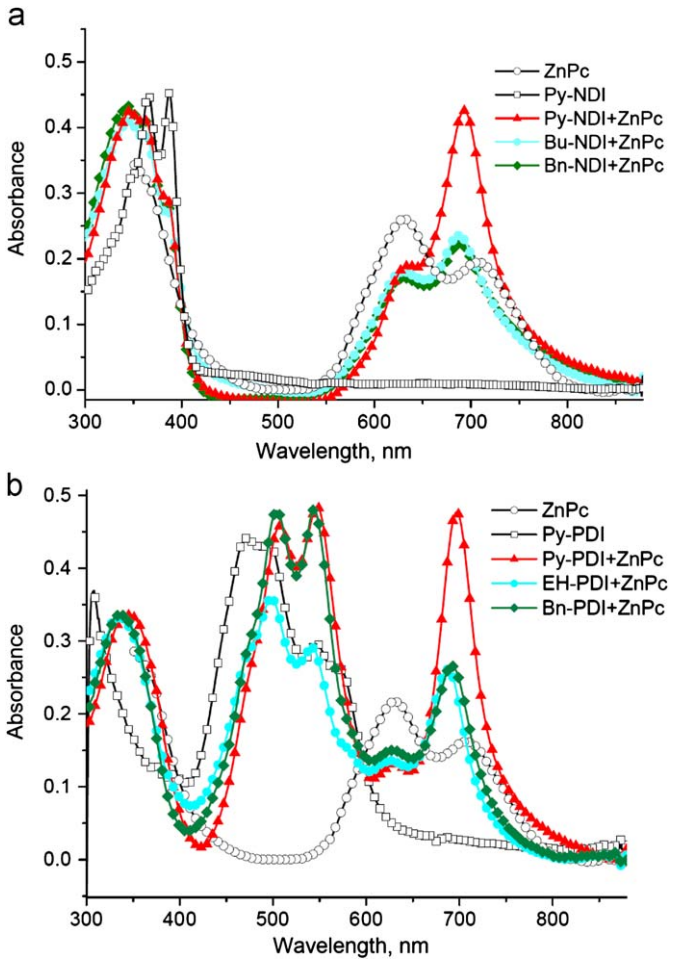

Fig. 3. Absorption spectra of pristine materials and co-evaporated thin films comprising ZnPc and different NDIs (a) or PDIs (b).

3.4. Photovoltaic performance of the ZnPc/NDI and ZnPc/PDI bilayer structures

We have fabricated simple bilayer and diffuse bilayer photovoltaic devices. In the case of bilayer devices, first 40 nm of the electron donor ZnPc were thermally evaporated in vacuum on a transparent ITO/PEDOT-PSS anode. Afterwards, 30 nm of NDI or PDI were evaporated as a top layer. At the end, 0.9 nm of LiF and 100 nm of Al were deposited in vacuum to produce a top electrode.

Diffusion bilayer devices were made by evaporation of 10 nm of pure ZnPc as bottom-layer followed by co-evaporation of ZnPc and PDI to yield a 45 nm thick composite interlayer and finally by deposition of 20 nm of pure PDI as a top layer. This three-layer photoactive system was sandwiched between ITO/PEDOT-PSS and LiF/Al electrodes. Schematic representations of the resulting photovoltaic cell architectures are shown in Fig. 4.

The *I–V* curves obtained for the photovoltaic devices comprising different electron acceptor materials are shown in Fig. 5. Short circuit current densities (I_{SC}), open circuit voltages (V_{OC}), fill factors (FF) and power conversion efficiencies (η) are listed in Table 2. We note that the devices fabricated here were not fully optimized and these performances most likely can be improved significantly.

The results show that Py-PDI and Py-NDI outperform strongly other materials in both bilayer and diffusion bilayer photovoltaic cells. It is most clearly seen from a comparison of the bilayer ZnPc/NDI and diffusion bilayer ZnPc/ZnPc:PDI/PDI devices where pyridyl-containing compounds show at least two times higher power conversion efficiencies than other materials (Table 2).

In contrast to Py-PDI/ZnPc devices, the light-on *I–V* curves for Bn-PDI/ZnPc cells have an S-shape behavior that suggests the existence of some counter diodes for charge transport in the system. Bilayer devices comprising ZnPc and other perylene diimides (EH-PDI and CyHex-PDI) yielded 5–20 times lower power conversion efficiencies than Py-PDI/ZnPc cells.

The fluorescence quenching experiments in solutions and absorption spectroscopy study of the co-evaporated composite films that we performed in this work suggest strongly a complex formation between ZnPc and Py-NDI or Py-PDI in solution and solid state. In addition, the shapes of the IPCE spectra (similar to optical spectra shown in Fig. 3) recorded for the diffusion bilayer cells suggests the complex formation between Py-PDI (Py-NDI) and ZnPc (see Supporting information). Therefore, we propose that such complex formation enhances strongly the electronic coupling between electron donor and electron acceptor materials that results in an improved photoinduced charge carrier generation in photovoltaic devices.

The IPCE spectra obtained for the investigated cells confirm such conclusion (Fig. 5). The highest values in the IPCE spectra were obtained for devices based on Py-NDI/ZnPc and Py-PDI/ZnPc material combinations. Py-PDI and Py-NDI as electron acceptor components provide more efficient photocurrent generation in photovoltaic cells in comparison with reference NDIs and PDIs possessing no chelating groups. It is somewhat surprising that a major fraction of photocurrent in ZnPc/PDI devices is generated from photons absorbed by ZnPc in the 550–800 nm region while the contribution from PDI at 400–550 nm is relatively weak. The only exception is the ZnPc/Bn-PDI system for which the contributions from PDI and ZnPc are relatively balanced.

It is also possible that the complex formation induces some ordering of donor and acceptor molecules with respect to each other in the bulk that provides pathways for transport of charges to the electrodes. In particular, such effects are suspected in diffuse bilayer devices where Py-PDI shows much better performance than Bn-PDI and EH-PDI (Table 2).

3.5. Transient photoresponse characteristics of ZnPc/Py-PDI bilayer devices

Good photochemical and environmental stability of MPc/PDI (M=Zn, Cu) material combinations makes promising their use in organic photodetectors. Spectral response of these photodetectors covers the whole visible range while high sensitivity can be achieved simply by applying appropriate bias voltages to the electrodes of the devices.

As example, we studied the transient photoresponse characteristics of a ZnPc/Py-PDI bilayer device without applying any bias voltage to the electrodes. First, the cell was irradiated by short (10 ns) light pulses from an ultraviolet nitrogen laser (337 nm). The device demonstrated a very quick photoresponse (1×10^{-6} s) with relatively slow decay (6×10^{-5} s, Fig. 6). Therefore, even under zero applied voltage (that means zero power consumption) the ZnPc/Py-PDI bilayer cells can give photoresponses with a frequency of 1.7×10^{5} Hz that is fast enough for many kinds of applications. For additional illustration, the investigated photovoltaic device was irradiated by short (2.5×10^{-4} s) light pulses from a blue light emitting diode with λ_{max}=460 nm. As can be seen from Fig. 6b, the photoresponse of the ZnPc/Py-PDI cell followed nicely the light modulation behavior demonstrating the potential of the Py-PDI/ZnPc and Py-NDI/ZnPc systems for use as photoactive materials in organic photodetectors.

ZnPc/Py-PDI and ZnPc/Py-NDI bilayer devices demonstrated relatively strong photoconductivities. For example, illuminated ZnPc/Py-NDI diodes under positive applied voltages of +1.0 – 1.5 V

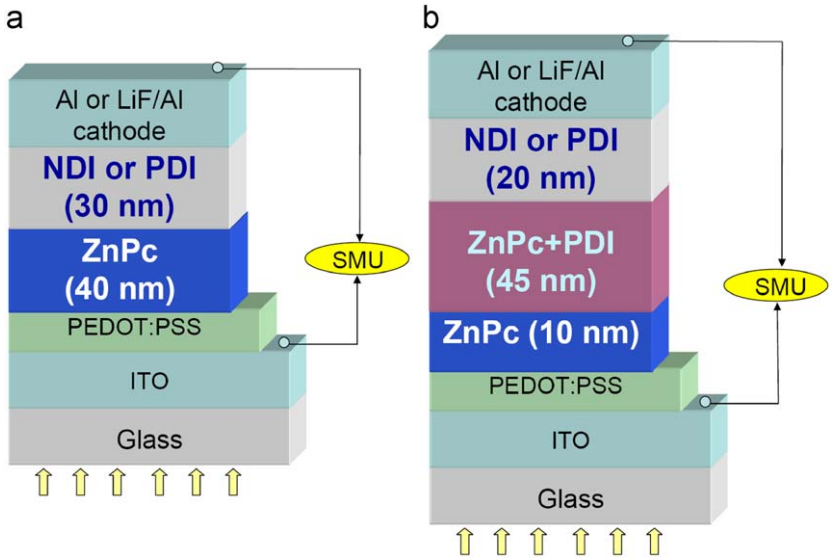

Fig. 4. Schematic layouts of simple bilayer (a) and diffusion bilayer (b) photovoltaic devices.

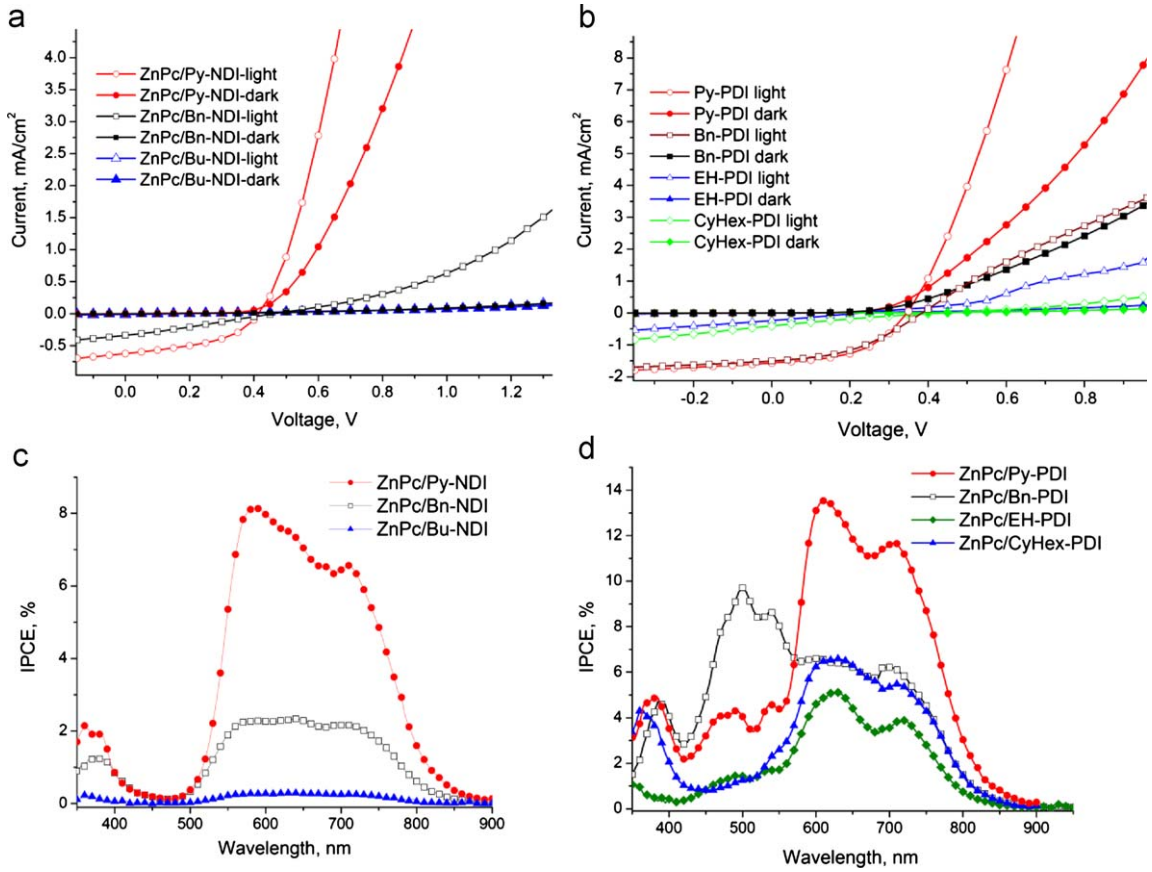

Fig. 5. *I–V* curves (a, b) and IPCE spectra (c, d) for bilayer cells comprising ZnPc/NDI (a, c) and ZnPc/PDI (b, d) material combinations.

show 2.5–3.0 times higher current densities than in the dark. Therefore these diodes can operate under forward bias.

A way to estimate the multiplication from the *I–V* characteristics is to take the difference between light and dark current at forward bias and divide it by the short circuit current. As the quantum efficiency corresponding to the short circuit current is measured in the IPCE, the IPCE spectrum multiplied by this factor is a rough approximation for the quantum efficiency spectrum under forward bias. The assumption taken here is that the IPCE spectrum does not change significantly under applied bias, which has been observed in similar systems [25].

According to these preliminary numerical estimations, photodiodes comprising ZnPc/Py-NDI system under applied forward bias voltage of 1.5 V would show external quantum efficiencies of ca.

Table 2
Output characteristics of photovoltaic devices comprising ZnPc and investigated PDI and NDI derivatives.

Active layer	I_{SC} (mA/cm^2)	V_{OC} (mV)	FF (%)	η (%)
Bilayer devices				
ZnPc/Py-PDI	1.57	350	48	0.3
ZnPc/Bn-PDI	1.51	380	42	0.2
ZnPc/CyHex-PDI	0.41	450	20	0.04
ZnPc/EH-PDI	0.24	200	29	0.01
ZnPc/Py-NDI	0.64	410	47	0.1
ZnPc/Bn-NDI	0.31	400	17	0.02
ZnPc/Bu-NDI	0.01	300	25	$\sim 7.10^{-4}$
Diffusion bilayer devices				
ZnPc/ZnPc+Py-PDI/Py-PDI	1.49	400	35	0.2
ZnPc/ZnPc+Bn-PDI/Bn-PDI	0.64	450	23	0.07
ZnPc/ZnPc+ EH-PDI/EH-PDI	0.75	500	25	0.1

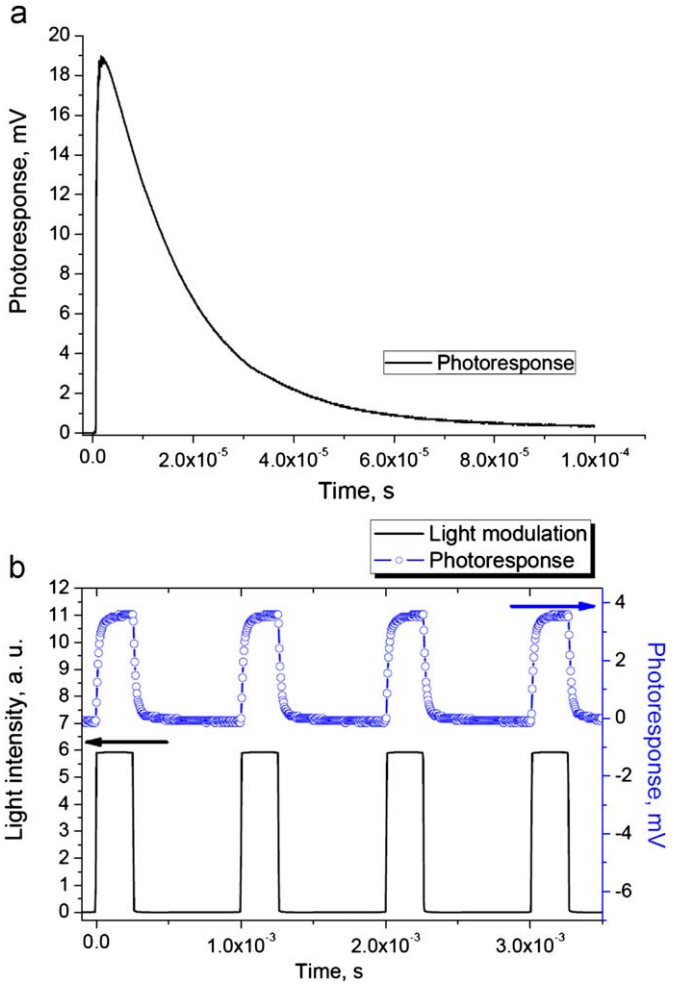

Fig. 6. The photoresponse of a ZnPc/Py-PDI bilayer cell induced by single 10 ns light pulse from a 337 nm nitrogen laser (a). Detection of the light from a 460 nm light emitting diode modulated with a 4 KHz frequency by the ZnPc/Py-PDI device (b).

400–500% between 600 and 800 nm. This makes the application of the developed material combinations promising for the design of high sensitivity organic photodetectors.

4. Conclusions

We designed novel electron acceptor materials Py-PDI and Py-NDI by modifying the perylene diimide or naphthalene diimide cores with chelating 3-pyridylmethyl substituents. These compounds show improved characteristics in organic photovoltaic devices, proposed to be due to their ability to form coordination complexes with the donor material ZnPc. The complex formation improves electronic coupling between electron donor and electron acceptor components that facilitates photoinduced charge carrier generation. The observed effect of the complex formation on the device performance might be very useful in designing new types of efficient small molecular organic photovoltaic cells. The combinations of Py-PDI and Py-NDI with ZnPc are considered as promising materials for organic photodetectors. In particular, a fast photoresponse (1×10^{-6} s) was demonstrated for the ZnPc/Py-PDI bilayer devices.

Acknowledgement

The authors thank Prof. A. S. Peregudov of A. N. Nesmeyanov Institute of Organoelement Compounds of RAS (Moscow, Russia) for the NMR spectra of the reported compounds. The financial support was provided by Russian Ministry of Science and Education (contract 02.513.11.3358), the Russian Foundation for Basic Research (07-04-01742-a, 10-03-00443a) and the Russian President Foundation (MK MK-4305.2009.3).

Appendix A. Supporting information

Supplementary data associated with this article can be found in the online version at doi:10.1016/j.solmat.2009.12.027.

References

[1] H. Hoppe, N.S. Sariciftci, Organic solar cells: an overview, J. Mater. Res. 19 (2004) 1924–1945.
[2] M. Helgesen, R. Søndergaard, F.C. Krebs, Advanced materials and processes for polymer solar cell devices, J. Mater. Chem. 20 (2010) 36–60.
[3] T. Ameri, G. Dennler, C. Lungenschmied, C.J. Brabec, Organic tandem solar cells: a review, Energy Environ. Sci. 2 (2009) 347–363.
[4] S.E. Shaheen, D.S. Ginley, G.E. Jabbour, Organic-based photovoltaics: toward low-cost power generation, MRS Bull. 30 (2005) 10–15.
[5] F.C. Krebs, M. Jørgensen, K. Norrman, O. Hagemann, J. Alstrup, T.D. Nielsen, J. Fyenbo, K. Larsen, J. Kristensen, A complete process for production of flexible large area polymer solar cells entirely using screen printing—first public demonstration, Sol. Energy Mater. Sol. Cells 93 (2009) 422–441.
[6] F.C. Krebs, S.A. Gevorgyan, J. Alstrup, A roll-to-roll process to flexible polymer solar cells: model studies, manufacture and operational stability studies, J. Mater. Chem. 19 (2009) 5442–5451.
[7] R. Koeppe, N.S. Sariciftci, Photoinduced charge and energy transfer involving fullerene derivatives, Photochem. Photobiol. Sci. 5 (2006) 1122–1131.
[8] D. Wohrle, D. Meissner, Organic solar cells, Adv. Mater. 3 (1991) 129.
[9] C.W. Tang, Two-layer organic photovoltaic cell, Appl. Phys. Lett. 48 (1986) 183.
[10] F.C. Krebs, Fabrication and processing of polymer solar cells: a review of printing and coating techniques, Sol. Energy Mater. Sol. Cells 93 (2009) 394–412.
[11] K. Walzer, B. Maennig, M. Pfeiffer, K. Leo, Highly efficient organic devices based on electrically doped transport layers, Chem. Rev. 107 (2007) 1233–1271.
[12] H. Gommans, D. Cheyns, T. Aernouts, C. Girotto, J. Poortmans, P. Heremans, Electro-optical study of subphthalocyanine in a bilayer organic solar cell, Adv. Funct. Mater. 17 (2007) 2653–2658.
[13] R. Koeppe, P.A. Troshin, R.N. Lyubovskaya, N.S. Sariciftci, Complexation of pyrrolidinofullerenes and zinc-phthalocyanine in a bilayer organic solar cell structure, Appl. Phys. Lett. 87 (2005) 244102.
[14] P.A. Troshin, R. Koeppe, A.S. Peregudov, S.M. Peregudova, M. Egginger, R.N. Lyubovskaya, N.S. Sariciftci, Supramolecular association of pyrrolidinofullerenes bearing chelating pyridyl groups and zinc phthalocyanine for organic solar cells, Chem. Mater. 19 (2007) 5363–5372.
[15] H.E. Katz, Z. Bao, S.L. Gilat, Synthetic chemistry for ultrapure, processable and high-mobility organic transistor semiconductors, Acc. Chem. Res. 34 (2001) 359–369.

[16] H. Tanaka, T. Yasuda, K. Fujita, T. Tsutsui, Transparent image sensors using an organic multilayer photodiode, Adv. Mater. 18 (2006) 2230–2233.
[17] T. Morimune, H. Kam, Y. Ohmori, High-speed organic photodetectors using heterostructure with phthalocyanine and perylene derivative, Jpn. J. Appl. Phys. 45 (2006) 546–549.
[18] P. Peumans, V. Bulovic, S.R. Forrest, Efficient, high-bandwidth organic multilayer photodetectors, Appl. Phys. Lett. 76 (2000) 3855–3857.
[19] T.Someya, Y. Kato, S. Iba, Y. Noguchi, T. Sekitani, H. Kawaguchi, T. Sakurai, Integration of organic FETs with organic photodiodes for a large area, flexible, and lightweight sheet image scanners, IEEE Trans. Electron. Dev. 52 (2005) 2502–2511.
[20] T. Morimume, H. Kajii, Y. Ohmori, Photoresponse properties of a high-speed organic photodetector based on copper-phthalocyanine under red light illumination, IEEE Photon. Technol. Lett. 18 (2006) 2662–2664.
[21] G. Valduga, E. Reddi, G. Jori, R. Cubeddu, P. Taroni, G. Valentini, Steady state and time-resolved spectroscopic studies on zinc(II) phthalocyanine in liposomes, J. Photochem. Photobiol. B 16 (1992) 331–340.
[22] R. Koeppe, P.A. Troshin, A. Fuchsbauer, R.N. Lyubovskaya, N.S. Sariciftci, Photoluminescence studies on the supramolecular interactions between a pyrollidinofullerene and zinc-phthalocyanine used in organic solar cells, Fuller. Nanotub. Carb. Nanostruc. 14 (2006) 441–446.
[23] P.A. Troshin, S.I. Troyanov, G.N. Boiko, R.N. Lyubovskaya, A.N. Lapshin, N.F. Goldshleger, Efficient [2+3] cycloaddition approach to synthesis of pyridinyl based [60]fullerene ligands, Fuller. Nanot. Carb. Nanostruct. 12 (2004) 435–441.
[24] M.E. El-Khouly, O. Ito, P.M. Smith, F. D'Souza, Intermolecular and supramolecular photoinduced electron transfer processes of fullerene–porphyrin/phthalocyanine systems, J. Photochem. Photobiol. C 5 (2004) 79–104.
[25] M. Egginger, R. Koeppe, F. Meghdadi, P. Troshin, R. Lyubovskaya, D. Meissner, N.S. Sariciftci, Proc. Soc. Photo-Opt. Instrum. Eng. 6192 (2006) 61921Y–619211.